Eur. Phys. J. Special Topics **145**, 35–47 (2007)

DOI: 10.1140/epjst/e2007-00146-3

THE EUROPEAN PHYSICAL JOURNAL SPECIAL TOPICS

Experiments with twisted light

Some of the mechanical and quantum-mechanical properties of optical vortices

J. Courtial[1,a] and K. O'Holleran[1]

[1]Department of Physics & Astronomy, University of Glasgow, Glasgow G12 8QQ, Scotland, UK

Abstract. The generic – that is, stable under perturbations – nodes of the field in a monochromatic light beam are optical vortices. We describe here their connection to Chladni's nodal lines in the oscillations of metal plates, as well as a few experiments that have been performed with optical vortices. We will describe how optical vortices can be generated experimentally; how it can be shown that they possess orbital angular momentum; how individual photons can be sorted according to their vortex state; and how optical vortices can be used to demonstrate higher-dimensional quantum entanglement.

1 Introduction

Ernst Chladni is well known for exciting sand-covered resonant oscillations of metal plates with a bow [1]. The sand accumulated in lines where the amplitude of the oscillation was zero – the nodal lines –, making them visible. This, in turn, excited many of Chladni's contemporaries, including Napoleon [2].

It is interesting to study the displacement of the plate from the equilibrium position, $A(x, y, t)$, near the nodal lines. In a complex notation, the actual displacement $A(x, y, t)$ is the real part of a complex amplitude $u(x, y) \exp(\mathrm{i}\omega t)$, where the exponential term describes the time evolution. The complex fields $u(x, y)$ in the neighbourhood of nodal lines along the x and y axis, respectively, is

$$u_x(x, y) = y \tag{1}$$

and

$$u_y(x, y) = x. \tag{2}$$

Frames (a) and (b) in figure 1 show snapshots of the corresponding displacements $A(x, y, t)$. In time, the displacement pivots around the nodal lines.

The resonant oscillations Chladni excited with his bow are, of course, eigenmodes of the plate. Each eigenmode has an oscillation frequency; if two have the same frequency, that is if they are frequency-degenerate, their superpositions are also eigenmodes. Often a nodal line of one frequency-degenerate eigenmode crosses that of the other. This is, for example, the case in circular plates, which can have a single nodal line through the centre (e.g. figure 105 from ref. [3], which is more easily accessible in ref. [4]): because of the symmetry of the plate, the nodal line can cross the centre at any angle without changing the eigenmode's oscillation frequency; specifically, two frequency-degenerate modes with nodal lines in the x and y direction, locally described by equations (1) and (2) are possible. What are the resulting oscillation structures near the crossing point?

[a] e-mail: j.courtial@physics.gla.ac.uk

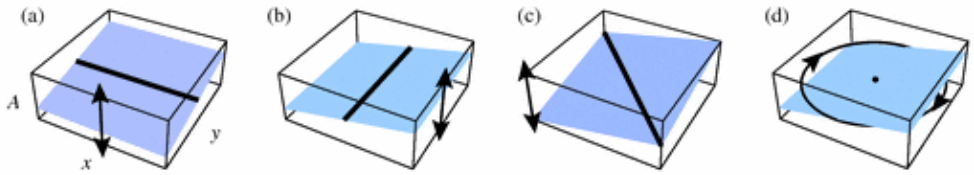

Fig. 1. Chladni lines and vortices. The figures show snapshots of a 2-dimensional amplitude field $A(x, y, t)$ – the displacement of a Chladni plate from its equilibrium position, but equally well the electric field in a light beam – that represent nodal lines in the y (a) and x direction (b) and simple superpositions of these. An in-phase superposition gives a nodal line at 45° (c), a superposition that is out of phase by $\pi/2$ results in a vortex (d). The time evolution of A near a nodal line is best described as pivoting around the nodal line; near a vortex, A rotates.

In the case of the complex fields corresponding to a nodal line in the x and y direction, respectively given by equations (1) and (2), simply being summed up, that is for

$$u(x, y) = x + y, \tag{3}$$

the resulting eigenmode contains a nodal line at 45° with respect to the x and y axes figure 1(c)); in time, the plate now pivots around a different line. If the two eigenmodes are added out-of-phase by $\pi/2$, that is if

$$u(x, y) = x + \mathrm{i}y, \tag{4}$$

the displacement from the equilibrium positions rotates around the intersection point (figure 1(d)) – at the intersection point the resulting superposition contains a vortex.

To the best of our knowledge, neither Chladni nor anybody else ever observed vortices in the motion of plates, which should manifest themselves on a Chladni plate as small islands of sand.[1] Vortices have, however, been predicted in eigenfunctions of highly symmetric quantum billiards [7–9]. Experimentally, the signatures of coherent excitations of standing waves – of which vortices are one particular example – have been seen in highly symmetric, closed, microwave cavities that are coherently excited at different points [10]. Vortices have been predicted to appear much more readily in quantum billiards without time-reversal symmetry [11], where they have in fact been seen experimentally [12–16].

The fields in open billiards are very similar to light beams travelling through a reflecting obstacle course. Vortices in light beams – optical vortices – are generic, that is, occuring in typical waves [17]: speckle fields, for example, are riddled with optical vortex structures [18].

As the generic oscillation-free features of light fields, optical vortices are the optical analogue of Chladni's nodal lines. But this analogy goes further: just like sand grains on a Chladni plate avoid areas of large oscillation and therefore accumulate in nodal lines, atoms in a blue-detuned laser beam (i.e. whose frequency is greater than that of a nearby atomic resonance) avoid high intensities and can accumulate in the vortex lines [19], as anticipated by Little [20].

Optical vortices were first described by Nye and Berry [21]. In a 3D light beam, they form lines of zero intensity [22]. In all of the experiments reviewed here the charge m of the optical vortices can take on a range of integer values. Higher-charge vortices (with $\|m\| > 1$) are non-generic: they are not stable with respect to almost all perturbations [23], which split a charge-m vortex into $\|m\|$ vortices of charge ± 1 (the sign is that of m). The complex field near the centre of a canonical charge-m vortex at the origin is of the form [24]

$$u(x, y) = (x \pm \mathrm{i}y)^{|m|} = \exp(im\phi), \tag{5}$$

[1] Confusingly, islands of very fine sand can preferentially accumulate at the anti-nodes of the oscillation [5] Perhaps Faraday observed vortices, though: Fig. 20 in Ref. [6] shows islands of sand to form at the intersections of nodal lines of a plate vibrating under water, but the nature of the plate oscillation around these islands is not clear.

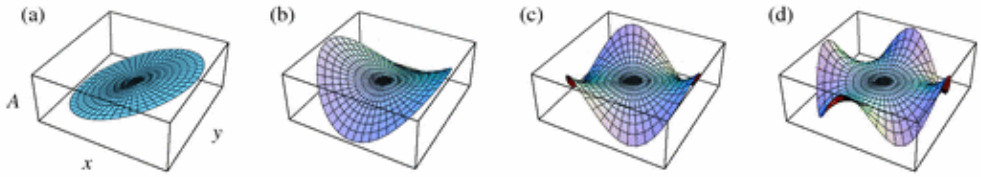

Fig. 2. Higher-charge vortices. The figures show snapshots of a 2-dimensional amplitude field $A(x, y)$ that represents vortices of charges $m = 1$ (a) to 4 (d). During one oscillation period the field rotates through an angle $360^\circ/m$, that is the field around a charge-1 vortex rotates through m times as fast as that around a charge-m vortex.

where the plus and minus sign respectively correspond to positive-m and negative-m vortices. Higher-charge vortices have also been predicted in quantum billiards [8].

An interesting exercise is plotting the time evolution of $A(x, y)$ – the electric field in a light field or the displacement from equilibrium of a Chladni plate – around higher-charge vortices. Figure 2 shows snapshots of $A(x, y)$ around vortices with charges m from 1 to 4: an inclined plane ($m = 1$), a saddle ($m = 2$), and higher-order saddles ($m = 3, 4$). The time evolution is a rotation around the vortex; in one optical period, $A(x, y)$ near a charge-m vortex rotates through $360^\circ/m$ (the sign of m determines the sense of rotation), so the field/displacement around higher-charge vortices rotates slower.

We review here a few of the many experiments performed with optical vortices, specifically the controlled creation of optical vortices (section 2), experiments relating to the orbital angular momentum associated with optical vortices (section 3), an interferometric scheme that sorts light beams into their vortex components (section 4), and the generation of photons that are entangled in their vortex state (section 5).

This article treats a few aspects of mostly scalar optical vortices in linear media. Other work on optical vortices, which has not been reviewed here, includes the propagation of optical vortices in non-linear media, where they can form solitons [25] and interact in other ways [26,27], and extensions to polarization singularities [28] and discrete vortices in lattices [29]. A much more complete overview of work related to optical vortices can be found in a recent review [30]; there is even a whole book on optical vortices [31]. Many review of related fields, for example on solitons [32,33] and optical tweezers [34], can also be helpful.

2 Making optical vortices

It is not difficult to create a light beam that contains vortices; for example, speckle, a gaussian random field easily recognisable to anyone who has worked with lasers, contains a complex network of optical vortices [35]. In isotropic random fields the probability of creating a positive-charge vortex and a negative-charge vortex is the same, so the sum of all the vortex charges is approximately zero. In fact it is difficult to create a light beam *without* vortices: any stray light (for example scattered light) interferes with the beam (in parts of beam of an intensity comparable to that of the stray light noticeably so), and even very simple interference can lead to optical vortices, as discussed in the following paragraph.

One way of analyzing light fields is in terms of their Fourier components: uniform plane waves. In this context, the simplest way to generate optical vortices is to interfere three uniform plane waves of the same intensity [36,37]. Figure 3(a) shows a cross-section through such a field. Vortex lines cross this plane at positions of complete destructive interference, which occurs on points that form a distorted honeycomb lattice. The vortices come in pairs with opposite charges, so the sum of the vortex charges of this field is again zero.

An optical vortex can be created in a controlled manner by directly imprinting its phase structure onto a light beam. Perhaps the most obvious method is introducing an azimuthally-varying optical path length by passing the light beam through a dielectric of azimuthally-varying thickness. Such a device is known as a spiral phase plate (SPP, Fig. 4(a)). Beijersbergen *et al.*

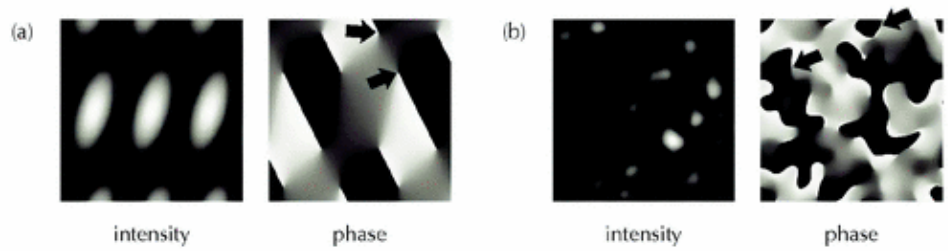

Fig. 3. Intensity and phase cross-sections created by the interference between 3 (a) and 300 (b) random plane waves. Phase is represented in grayscale, ranging from black (phase 0) to white phase 2π. Vortices can be identified either as points of zero intensity or as singular points in the phase, that is points at which all phases meet; a few examples are marked by arrows. Depending on the vortex charge, the phase can be seen to increase clockwise ($m = +1$) or anti-clockwise ($m = -1$) around the vortices.

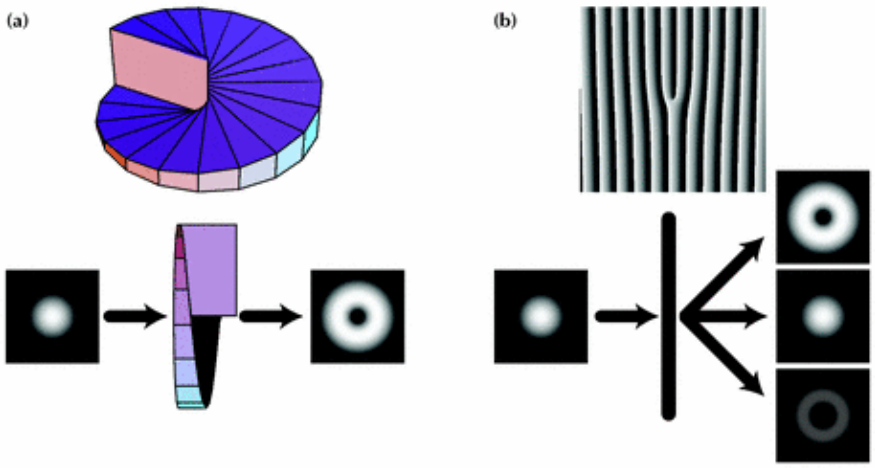

Fig. 4. Two methods of producing a vortex in a controlled manner. (a) A spiral phase plate (SPP; top) – dielectric material of azimuthally-varying thickness – can introduce a phase term of the form $m\phi$ by path difference. A SPP transforms a Gaussian beam into a beam with a central vortex (bottom). (b) Phase holograms also introduce such a phase term. The addition of a blazed grating – the phase hologram of a wedge – results in a distinctive phase pattern in the shape of a forked grating (top; grayscale representation). It splits the light into different grating orders, whereby only the +1st order possesses the desired phase profile. In the case of a hologram introducing a phase of the form $m\phi$, the nth order has a vortex of charge $m \cdot n$ (bottom).

were the first to generate an optical vortex using a SPP [38]. Machining a SPP for visible light is no mean task: the first SPP used at optical frequencies involved a step height of 0.7 mm, but also required to be immersed in a surrounding liquid whose refractive index was tuned to achieve a phase difference of $2\pi m$ (the refractive index difference between the liquid and SPP was of order 10^{-3}). Machining of SPPs in the optical regime to work in air has been achieved much more recently [39,40].

Another method of imprinting the correct phase structure is to use a computer-generated phase hologram (that is, the phase pattern has been calculated by a computer) of a SPP (Fig. 4(b)) [41,42]. The basic phase pattern of such a hologram imprints is simply of the form $m \cdot \phi$ (where ϕ is the azimuthal angle). However, in order to avoid problems with the phase response of a phase hologram, phase holograms are often calculated such that the desired beam diffracts at an angle from the illuminating beam, resulting in a phase pattern in the shape of a forked grating (figure 4(b)). Due to the relative ease of manufacturing a hologram,

the holographic method actually precedes the successful use of a SPP. Computer-generated holograms may either be printed on photographic film and subsequently bleached to convert different grayscale levels into corresponding phase delays; or they may be displayed on a spatial light modulator (SLM), which can be configured either as a phase hologram or as an intensity hologram. Printed holograms achieve much higher resolutions and diffraction efficiencies (typically 90% compared to 40%). However, SLMs are becoming increasingly common in optics laboratories as they can be computer-controlled in real time to act as arbitrary holograms.

It is also possible to convert a higher-order Hermite-Gauss mode into a corresponding Laguerre-Gauss mode with a central vortex. This can be achieved by passing the Hermite-Gaussian beam through a cylindrical-lens mode converter whose parameters have been matched to the beam's waist size [43].

The controlled generation of vortices discussed so far results in straight vortex lines. Vortices can also be shaped into other topological structures such as links and knots [44]. The recipe for creating such structures involves creating superpositions of either high-order Bessel or Laguerre-Gauss modes and then perturbing these with a plane wave. Vortex links and knots were realised experimentally by using an SLM to control both the phase and intensity structure of the beam in order to create the required superposition of Laguerre-Gauss modes [45].

3 Optical vortices and light's orbital angular momentum

The time evolution of the field in the neighbourhood of a canonical optical vortex is a rotation of the phase structure around the vortex (the intensity is radially symmetric). Like most rotations, this one is associated with angular momentum, namely the orbital angular momentum (OAM) of light [46].

In 1992, Allen and co-workers [47] observed that the complex field describing Laguerre-Gauss beams,

$$u(r,\phi) \propto R(r)\exp(-\mathrm{i}m\phi), \tag{6}$$

which contains a charge-m optical vortex line along the z axis, is an eigenstate of the orbital angular momentum operator

$$\hat{L}_z = -\mathrm{i}\hbar\frac{\partial}{\partial\phi} \tag{7}$$

with eigenvalues $m\hbar$. By analogy with quantum mechanics, they argued, such a beam should have an orbital angular momentum of $m\hbar$ per photon. (The same result can also be reached through a semi-classical argument [48].)

In 1995, the prediction that light can carry OAM was confirmed experimentally when He *et al.* succeeded in transferring angular momentum from a light beam to a microscopic particle trapped near the focus of that beam, thereby making the particle rotate [49]. OAM transfer to optically trapped particles was subsequently used to confirm the OAM content of light beams of the form (6) quantitatively, first by direct comparison with the spin of $\pm\hbar$ per photon [50], then by quantitative measurements of rotation rates [51].

An interesting aspect of the angular momentum of light is that it can give insights into the nature of spin and orbital angular momentum. In light in spin eigenstates, the electric-field vector at every point rotates on the spot; in light beams in OAM eigenstates, the phase structure of the entire beam rotates around the axis of the beam. When the two forms of angular momentum are transferred to microscopic particles, spin causes the particles to spin, that is to rotate on the spot, [52] while OAM causes them to orbit the beam axis [53].

4 Sorting individual photons according to their vortex state

The holographic techniques described above work also in reverse to split a light beam into its optical-vortex components. They even work for measuring the vortex charge of single photons [54], but not very efficiently: if a beam of photons is prepared to be, with equal probability, in

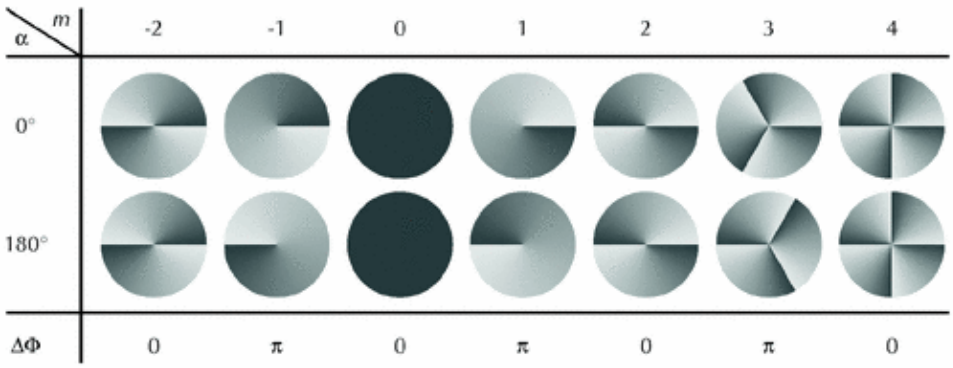

Fig. 5. Phase change resulting from rotation of vortex-phase patterns through 180°. The top row shows the charge, m, of the vortex. The second and third row respectively shows the corresponding phase pattern (grayscale representation) non-rotated ($\alpha = 0°$) and rotated through $\alpha = 180°$. The phase difference between the rotated and non-rotated beams is shown in the bottom row.

one of N different vortex states, the above holographic approach yields a definite result only for a fraction $1/N$ of the photons [55] (assuming 100% efficiency of all optical components).

An interferometric alternative that yield a definitive result for every photon (again assuming 100% efficiency of all optical components) was demonstrated in ref. [55]. This technique is now frequently cited, for example in the context of quantum computing (e.g. [56]) and quantum cryptography (e.g. [57,58]).

Consider a light beam with a cylindrically symmetric intensity and a central charge-m vortex, i.e. that is of the form

$$u(r, \phi) = R(r) \exp(\mathrm{i}m\phi). \tag{8}$$

The radial dependence is not important in this section; we choose here $R(r) \equiv 1$. Figure 5 shows examples of the transverse phase cross-sections of such beams for various values of m, and investigates the effect of a 180° rotation around the beam axis. When the $m = 1$ beam is rotated through 180° around its axis, the field at each point in the beam is out of phase with the un-rotated beam. In contrast, when a beam with charge $m = 2$ is rotated through 180° around its axis, the phase at every point is the same in the rotated and un-rotated beams.

The above behaviour of the $m = 1$ beam is representative of all pure vortex components with odd values of m; the behaviour of the $m = 2$ beam represents all pure vortex components with even m-values. It can be used in a 2-arm interferometer in which the beams in the two arms are rotated with respect to each other to separate even from odd vortex components in a light beam. The beam rotation can be achieved using Dove prisms to reflect the beam cross section twice with respect to different axes; figure 6 demonstrates how two successive reflections result in a rotation. (Note that Dove prisms do not simply reverse the handedness of light beams when the light beams are highly focussed [59].) Because of subtle additional phase differences in the beam splitters, light interfering constructively in one exit of the interferometer interferes destructively in the other. So any calculations of phase difference between the beams in the two arms of the interferometer apply only to one particular exit of the interferometer; in the other exit, the role of constructive and destructive interference is reversed. In the context of vortex-charge sorting, this means that an interferometer that rotates the beam in one arm of the interferometer by 180° with respect to that in the other leads to all even-charge vortices leaving the interferometer at one exit, while all the odd-charge vortex components leave the interferometer at the other exit (provided the path differences are adjusted correctly.) Such a Dove-prism interferometer [55] is shown in figure 7(a); results are shown in figure 8(a).

With interferometers in which the beams in the two arms are rotated with respect to each other not by 180°, as in the even-odd-m sorter, but through $\alpha = 90°$, the beams can be sorted further. Figure 9 shows the phase shift resulting from rotation of vortices with various charges

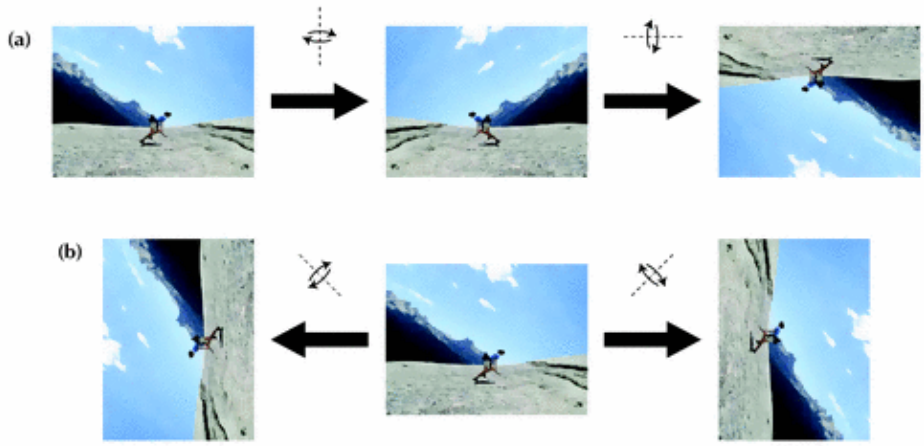

Fig. 6. Examples of rotation through reflections. (a) Successive reflections of the image on the left, first with respect to a vertical axis and then with respect to a horizontal axis, results in rotation through $\alpha = 180°$. Generally, successive reflections with respect to two axes that are rotated by an angle $\alpha/2$ (in the example shown $\alpha/2 = 90°$) result in a rotation through α. (b) Reflection of the center image with respect to an axis inclined by $-45°$ with respect to the horizontal (left) results in an image that is rotated by $180°$ compared to the image resulting from reflection of the center image with respect to an axis inclined by $+45°$ with respect to the horizontal (right). Generally, reflection with respect to one axis results in an image rotated by α relative to the image resulting from reflection with respect to an axis rotated by $\alpha/2$ with respect to the first axis.

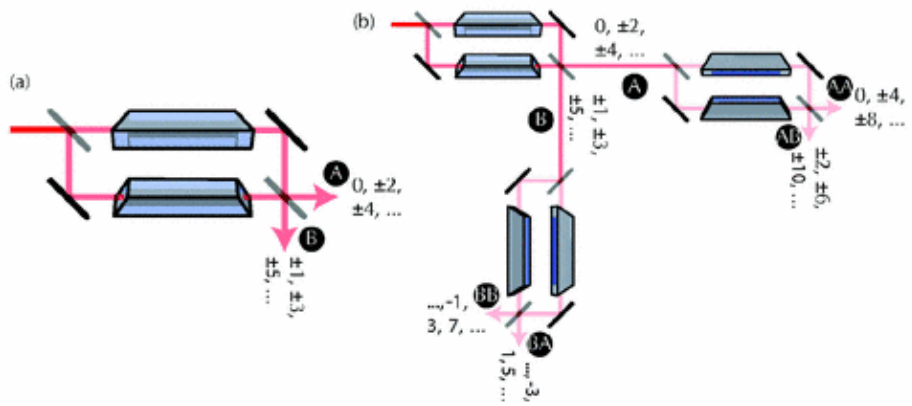

Fig. 7. Dove-prism interferometer for even-odd sorting (a) and Dove-prism-interferometer tree for further sorting (b). In the interferometer for odd-even sorting ((a) and top left interferometer in (b)), the two Dove prisms are rotated with respect to each other by $90°$, resulting in the beams in the two arms to be rotated with respect to each other by $180°$. If the path lengths are adjusted correctly, all beams with even m values leave the interferometer through exit A, those with odd m values through exit B. The additional two interferometers in (b) each rotate the beams in the two arms by $90°$ with respect to each other; if the path lengths are again adjusted correctly (and differently in the two interferometers), the right-hand interferometer sorts even-charge beams into integer and half-integer multiples of 4 ($m \bmod 4 = 0$, i.e. $m = 0, \pm 4, \pm 8, \ldots$, and $m \bmod 4 = 2$, i.e. $m = \pm 2, \pm 6, \ldots$, respectively), the bottom interferometer sorts odd-charge beams into the classes $m \bmod 4 = 1$ and $m \bmod 4 = 3$.

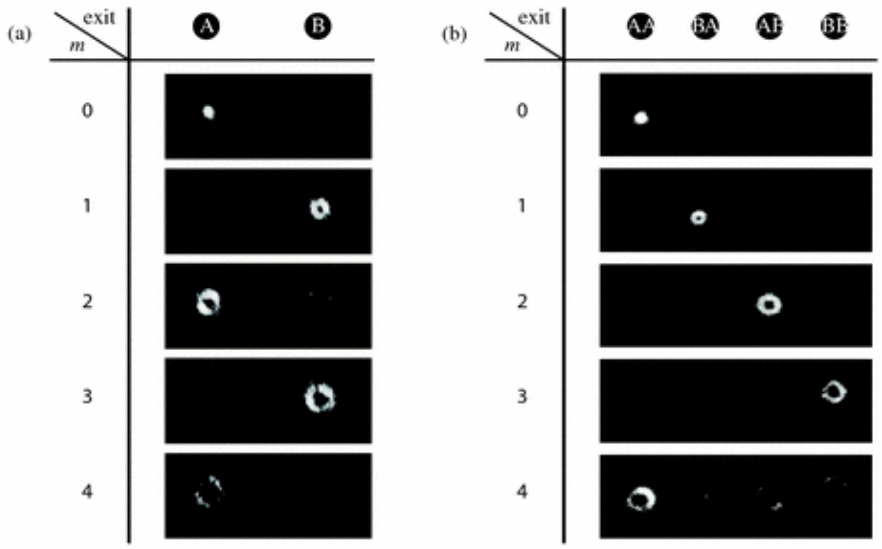

Fig. 8. Experimental results of vortex-charge sorting according to even ($m \bmod 2 = 0$) or odd ($m \bmod 2 = 0$) values of m (a) and according to $m \bmod 4 = 0, 1, 2, 3$. The columns show the intensity in each interferometer exit (see figure 7). The even-odd sorting was performed at single-photon level. (From ref. [55].)

through 90°. It can be seen that even-charge vortices suffer either a 0 or π phase shift, translating into constructive or destructive interference in an interferometer that rotates the beams in the two arms through 90° with respect to each other and in which the pathlength is the same. This is, in fact, how even-charge vortices can be sorted further into integer and half-integer multiples of 4 [55] (right-hand interferometer in figure 7(b)). Figure 9 also shows that odd-charge vortices suffer either a $\pi/2$ or $3\pi/2$ phase shift. In an interferometer, these phase differences can be turned into 0 and π through the introduction of an additional phase-shifting element [55] or simply path-length difference [60]; the bottom interferometer in figure 7(b) sorts odd-charge vortices like this. Experimental results of such sorting into four different classes are shown in figure 8(b). Further sorting into arbitrarily many classes is possible and described in references [55,60].

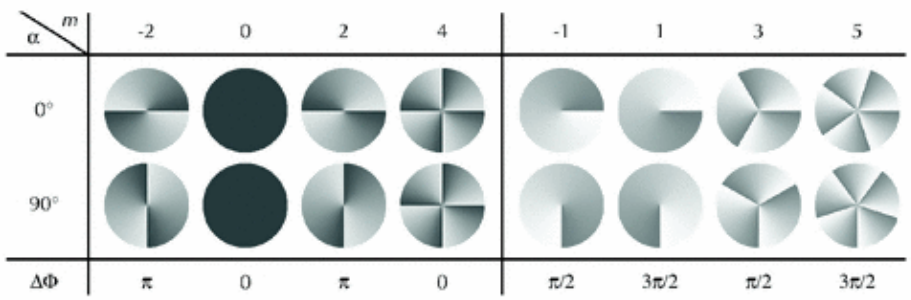

Fig. 9. Rotation of the phase patterns of even-charge (left block) and odd-charge (right block) vortices through 90°. In the case of the odd-charge vortices, the non-rotated ($\alpha = 0°$) and rotated ($\alpha = 90°$) patterns are globally out of phase by either $\Delta\Phi = \pi/2$ (for $m \bmod 4 = 3$, i.e. $m = \ldots, -5, -1, 3, 7, \ldots$) or $3\pi/2$ (for $m \bmod 4 = 3$, i.e. $m = \ldots, -3, 1, 5, 9, \ldots$); phase-shifting the rotated patterns by an additional $-\pi/2$ makes these phase differences either 0 or π [60].

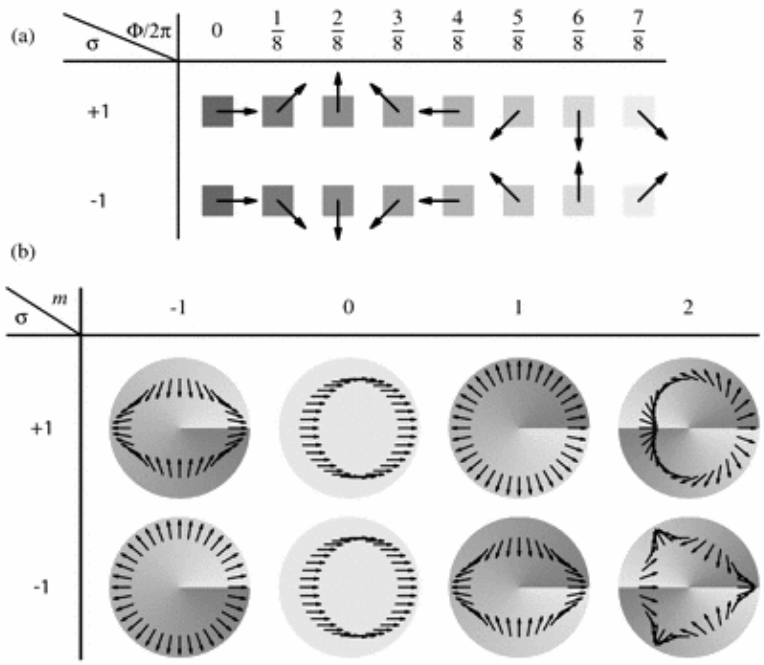

Fig. 10. Circularly polarized optical vortices. (a) Correspondence between phase (grayscale of square) and electric field vector for left- and right-hand circular polarization ($\sigma = \pm 1$); (b) Polarization patterns in circularly polarized vortices with charges $m = -1, 0, 1, 2$. Pictures after [61].

The ideas described above have also been applied to sort other types of vortices. Polarization vortices (fig.10) have been sorted experimentally using interferometers that rotate not only the phase- and intensity structure, but also the polarization direction [62], and a scheme to sort vortices in BECs has been examined theoretically [63].

5 Entangling optical vortices

Non-physicists do not have a problem with non-locality: why should there not be some form of instantaneous action at a distance? For most physicists the answer is simple: because Einstein's theory of special relativity [64], formulated in 1905, places an upper limit, namely the speed of light, c, on the speed with which the information about any "action" spreads.

This speed limit formed the basis of the Einstein-Podolsky-Rosen paradox [65], one of Einstein's objections to quantum mechanics. Einstein, Podolsky and Rosen noticed in 1935 that quantum mechanics allows a measurement in one place to have an immediate effect elsewhere, and concluded that [65] "the description of reality as given by a wave function is not complete", preferring instead a "hidden-variable" interpretation of quantum mechanics. In 1964, Bell [66] showed that any local, deterministic, structure underlying quantum mechanics implies that certain measurable quantities obey inequalities, now known as Bell's inequalities. In 1969, Clauser, Horne, Shimony and Holt [67] suggested an explicit experimental realization, using the polarization of pairs of photons, for a test of Bell's inequalities. In 1981, Aspect, Grangier and Roger [68,69] actually performed such an experiment. This experiment has since been refined in a number of ways (e.g. [70,71] – see Ref. [72] for a good review).

Such an experiment typically creates pairs of photons travelling in different directions. Aspect *et al.* triggered a cascade of two atomic transitions in a beam of Calcium atoms, whereby each of the two transitions emitted one photon. Most modern experiments use

non-linear crystals. If the two photons happen to be emitted in certain directions, they are collected into different arms of the setup, where they are sent through an analyzer and detected by a single-photon detector. The rate at which a detector registers photons is called the single-count rate. Photons belonging to the same pair are identified by a simultaneous "click" in the single-photon detectors in both arms; this is established through an electronic circuit counting signals that arrive within a very short time of each other. The number of coincidence counts per time is called the coincidence-count rate.

A modern experiment that uses a type-I phase-matched crystal might then record the following results. The single-count rate in each arm is independent of whether the analyzer is aligned in the vertical or horizontal direction. This implies that the photons in the arms are sometimes vertically polarized, and sometimes horizontally polarized. If the analyzers in the two arms are parallel, there is a high coincidence rate; if the analyzers are perpendicular, the coincidence rate is almost zero. This implies that the polarizations of the photons in the two arms are always the same.

This result could be interpreted in the following way: when they are created, the two photons take on the same linear polarization; the direction that common linear polarization is randomly chosen to be either vertical or horizontal. In other words, there is an explanation in terms of classical physics for the correlation between the photons. The polarizations have to be either vertical or horizontal, as photons linearly polarized at 45°, for example, are in an equal superposition of vertical and horizontal linear superposition. If any of the photons were polarized at 45°, they would pass through the analyzer in either vertical or horizontal direction with 50% probablity, a result that is not compatible with the near-zero coincidence rate measured for perpendicular analyzers.

However, the experiment also gives the following results when the analyzers in the two arms are aligned at ±45° with respect to the horizontal. First of all, the single-photon count rate in the arms is independent of the angle of the analyzer not only for 0° and 90°, but also all other angles, suggesting that the photons are not exclusively vertically or horizontally polarized. This contradiction is supported by the behaviour of the coincidence-count rate: whatever the angle of the analyzers in the two arms, if they are parallel the coincidence-count rate is high; if they are perpendicular, it is close to zero.

Clearly, the above interpretation of the first set of results needs to be revised. The interpretation provided by entanglement is that the polarization directions of the two photon are not decided when they are created, but as soon as one of the polarization direction of one of the photons is measured, that of the other photon *immediately* becomes the same. The measurement of one photon has a non-local effect, which appears to be in contradiction with Einstein's speed limit.

The above account contains a number of simplifications; for example, it completely ignores the efficiency of the single-photon detectors and the dark-count rate, and it arrives at the conclusion that the second photon is affected *immediately* without justification. Such objections to the entanglement interpretation have been addressed in a number of other experiments; Ref. [71], for example, spatially separates the polarization detection in the two arms to confirm the non-locality of the interaction.

The argument can be extended in another direction: from quantum variables that are described in a two-dimensional Hilbert space to those that are described in a N-dimensional space. The motivation for doing so derives for example from the desire to increase the information capacity of quantum communication [57,58], or – as pointed out in the paper of the same name [73] – from the fact that "Violations of Local Realism by Two Entangled N-Dimensional Systems Are Stronger than for Two Qubits".

Multi-dimensional entanglement was first demonstrated with different vortex states of light by Mair *et al.* [54], following theoretical suggestions [74,75]. Mair and colleagues used a type-I down-conversion crystal to generate photon pairs, and holograms of SPPs with single-photon detectors to measure the vortex state of both photons. They performed their experiment in two stages analogous to the two sets of results discussed above. First they demonstrated that the vortex states of the two photons are correlated: in the simplest case, that of a charge-0 pump beam, the vortex charge of the two down-converted photons is always opposite. This was

established for three different vortex charges. More generally, the orbital angular momentum is conserved in the down-conversion process. Then they demonstrated that the correlation cannot be explained in terms of classical physics. This was demonstrated by measuring the photons in a basis of superpositions of vortex states. Again, the superpositions were always correlated.

The pioneering work by Mair *et al.* has since been extended in a number of ways. Vaziri and colleagues, for example, demonstrated entanglement concentration [76], which is important for quantum communications, and Oemrawsingh and colleagues showed that photons could also be entangled in fractional vortex charges [77].

These experiments demonstrate a violation of generalized Bell's inequalities and pave the way for more powerful quantum communication. It should be pointed out that, even though the measurement of the state of an entangled photon produces a non-local effect, this does not allow information transfer at speeds greater than the speed of light [72].

6 Conclusions

Optical vortices are simply the zeros of optical fields. Considering this essential nothingness of optical vortices, research into optical vortices has developed in surprisingly diverse and fruitful ways, some of which we have described here. Michael Berry expressed this eloquently in the first part of the title of a paper [22]: "Much ado about nothing".

Thanks to Mark Dennis and Hans-Juergen Stoeckmann for discussions on the relationship between Chladni's nodal lines and vortices. KO'H is supported by the UK's Engineering and Physical Sciences Research Council (EPSRC), JC is supported by a Royal Society University Research Fellowship.

References

1. E.F.F. Chladni, *Entdeckungen über die Theorie des Klanges* (Breitkopf und Härtel, Leipzig, Germany, 1787)
2. T.D. Rossing, Am. J. Phys. **50**, 271 (1982), http://link.aip.org/link/?AJP/50/271/1
3. E.F.F. Chladni, *Die Akustik* (Breitkopf und Härtel, Leipzig, Germany, 1802)
4. M.D. Waller, Proc. Phys. Soc. **50**, 83 (1938), http://stacks.iop.org/0959-5309/50/83
5. J.R. Comer, M.J. Shepard, P.N. Henriksen, R.D. Ramsier, Am. J. Phys. **72**, 1345 (2004), http://link.aip.org/link/?AJP/72/1345/1
6. M. Faraday, Phil. Trans. Roy. Soc. Lond. **121**, 299 (1831), http://www.journals.royalsoc.ac.uk/link.asp?id=25m2674841600 6t6
7. Y.F. Chen, K.F. Huang, Y.P. Lan, Phys. Rev. E **66**, 066210 (2002), http://link.aps.org/abstract/PRE/v66/e066210
8. Y.F. Chen, K.F. Huang, Phys. Rev. E (Statistical, Nonlinear, and Soft Matter Physics) **68**, 066207 (2003), http://link.aps.org/abstract/PRE/v68/e066207
9. Y.F. Chen, K.F. Huang, J. Phys. A: Math. Gen. **36**, 7751 (2003), http://stacks.iop.org/0305-4470/36/7751
10. C. Dembowski, B. Dietz, H.D. Graf, A. Heine, F. Leyvraz, M. Miski-Oglu, A. Richter, T.H. Seligman, Phys. Rev. Lett. **90**, 014102 (2003), http://link.aps.org/abstract/PRL/v90/e014102
11. M.V. Berry, M. Robnik, J. Phys. A: Math. Gen. **19**, 1365 (1986), http://stacks.iop.org/0305-4470/19/1365
12. L.F. Chibotaru, A. Ceulemans, V. Bruyndoncx, V.V. Moshchalkov, Phys. Rev. Lett. **86**, 1323 (2001), http://link.aps.org/abstract/PRL/v86/p1323
13. M. Barth, H.J. Stöckmann, Phys. Rev. E **65**, 066208 (2002), http://link.aps.org/abstract/PRE/v65/e066208
14. K.F. Berggren, A.F. Sadreev, A.A. Starikov, Phys. Rev. E **66**, 016218 (2002), http://link.aps.og/abstract/PRE/v66/e016218
15. O. Olendski, L. Mikhailovska, Phys. Rev. E **67**, 056625 (2003), http://link.aps.org/abstract/PRE/v67/e056625

16. A.F. Sadreev, K.F. Berggren, Phys. Rev. E (Statistical, Nonlinear, and Soft Matter Physics) **70**, 026201 (2004), http://link.aps.org/abstract/PRE/v70/e026201
17. M. Berry, in *Les Houches Lecture Series Session XXXV*, edited by R. Balian, M. Kléman, J.P. Poirier (North-Holland, Amsterdam, 1981), pp. 453–543
18. M.V. Berry, J. Phys. A: Math. Gen. **11**, 27 (1978), http://stacks.iop.org/0305-4470/11/27
19. A. Kaplan, N. Friedman, N. Davidson, J. Opt. Soc. Am. B **19**, 1233 (2002)
20. W. Little, J. Appl. Phys. **43**, 2901 (1972), http://link.aip.org/link/?JAP/43/2901/1
21. J.F. Nye, M.V. Berry, Proc. R. Soc. Lond. A **336**, 165 (1974)
22. M.V. Berry, *Much ado about nothing: optical dislocation lines (phase singularities, zeros, vortices...)* in *Singular optics*, edited by M.S. Soskin, Proc. SPIE **348**, 7 (1998)
23. I. Freund, Opt. Commun. **159**, 99 (1999)
24. G. Molina-Terriza, J. Recolons, J.P. Torres, L. Torner, E.M. Wright, Phys. Rev. Lett. **87**, 023902 (2001), http://dx.doi.org/10.1103/PhysRevLett.87.023902
25. J.G.A. Swartzlander, C.T. Law, Phys. Rev. Lett. **69**, 2503 (1992), http://dx.doi.org/10.1103/PhysRevLett.69.2503
26. I.V. Basistiy, V.Y. Bazhenov, M.S. Soskin, M.V. Vasnetsov, Opt. Commun. **103**, 422 (1993)
27. J. Arlt, K. Dholakia, L. Allen, M.J. Padgett, Phys. Rev. A **59**, 3950 (1999)
28. I. Freund, Opt. Commun. **199**, 47 (2001)
29. D.N. Christodoulides, F. Lederer, Y. Silberberg, Nature **424**, 817 (2003)
30. A.S. Desyatnikov, L. Torner, Y.S. Kivshar, in *Progress in Optics 47*, edited by E. Wolf (North-Holland, Amsterdam, Amsterdam, 2005), pp. 219–319, http://arxiv.org/abs/nlin.PS/0501026
31. M. Vasnetsov, K. Staliunas, (eds.) *Horizons in World Physics, Vol. 228: Optical Vortices* (Nova Science Publishers, Huntington, NY, 1999)
32. Y.S. Kivshar, B. Luther-Davies, Physics Reports **298**, 81 (1998), http://dx.doi.org/10.1016/S0370-1573(97)00073-2
33. Y.S. Kivshar, G.P. Agrawal, *Optical Solitons: From Fibers to Photonic Crystals* (Academic Press, San Diego, CA, 2003)
34. J.E. Molloy, M.J. Padgett, Contemp. Phys. **43**, 241 (2002)
35. M.V. Berry, M.R. Dennis, Proc. R. Soc. Lond. A **456**, 2059 (2000)
36. K. O'Holleran, M.J. Padgett, M.R. Dennis, Opt. Express **14**, 3039 (2006), http://www.opticsinfobase.org/abstract.cfm?URI=oe-14-7-3039
37. K. O'Holleran, M.R. Dennis, M.J. Padgett, J. Eur. Opt. Soc. – Rapid Publications **1**, 06008 (2006)
38. M.W. Beijersbergen, R.P.C. Coerwinkel, M. Kristensen, J.P. Woerdman, Opt. Commun. **112**, 321 (1994)
39. S.S.R. Oemrawsingh, J.A.W. van Houwelingen, E.R. Eliel, J.P. Woerdman, E.J.K. Verstegen, J.G. Kloosterboer, G.W. 't Hooft, Appl. Opt. **43**, 688 (2004)
40. S.S.R. Oemrawsingh, E.R. Eliel, J.P. Woerdman, E.J.K. Verstegen, J. Kloosterboer, G.W. t'Hooft, J. Opt. A: Pure Appl. Opt. **6**, S288 (2004), http://www.ingentaconnect.com/content/iop/jopta/2004/00000006/00000005/art00029
41. V.Y. Bazhenov, M.V. Vasnetsov, M.S. Soskin, JETP Lett. **52**, 429 (1990)
42. N.R. Heckenberg, R. McDuff, C.P. Smith, A.G. White, Opt. Lett. **17**, 221 (1992)
43. M.W. Beijersbergen, L. Allen, H.E.L.O. van der Veen, J.P. Woerdman, Opt. Commun. **96**, 123 (1993)
44. M.V. Berry, M.R. Dennis, Proc. R. Soc. Lond. A **457**, 2251 (2001)
45. J. Leach, M. Dennis, J. Courtial, M. Padgett, Nature **432**, 165 (2004)
46. L. Allen, M.J. Padgett, M. Babiker, in *Progress in Optics XXXIX*, edited by E. Wolf (Elsevier Science B. V., New York, 1999), pp. 291–372
47. L. Allen, M.W. Beijersbergen, R.J.C. Spreeuw, J.P. Woerdman, Phys. Rev. A **45**, 8185 (1992)
48. G.A. Turnbull, D.A. Robertson, G.M. Smith, L. Allen, M.J. Padgett, Opt. Commun. **127**, 183 (1996)
49. H. He, M.E.J. Friese, N.R. Heckenberg, H. Rubinsztein-Dunlop, Phys. Rev. Lett. **75**, 826 (1995), http://link.aps.org/abstract/PRL/v75/p826
50. N.B. Simpson, L. Allen, M.J. Padgett, J. Mod. Opt. **43**, 2485 (1996)
51. V. Garces-Chavez, D. McGloin, M.J. Padgett, W. Dultz, H. Schmitzer, K. Dholakia, Phys. Rev. Lett. **91**, 093602 (2003), http://link.aps.org/abstract/PRL/v91/e093602
52. M.E.J. Friese, T.A. Nieminen, N.R. Heckenberg, H. Rubinsztein-Dunlop, Nature **394**, 348 (1998), http://dx.doi.org/10.1038/28566
53. A.T. O'Neil, I. MacVicar, L. Allen, M.J. Padgett, Phys. Rev. Lett. **88**, 53601 (2002),
54. A. Mair, A. Vaziri, G. Weihs, A. Zeilinger, Nature **412**, 313 (2001)

55. J. Leach, M.J. Padgett, S.M. Barnett, S. Franke-Arnold, J. Courtial, Phys. Rev. Lett. **88**, 257901 (2002)
56. A.N. de Oliveira, S.P. Walborn, C.H. Monken, J. Opt. B: Quantum Semiclass. Opt. **7**, 288 (2005), http://stacks.iop.org/1464-4266/7/288
57. A. Vaziri, G. Weihs, A. Zeilinger, Phys. Rev. Lett. **89**, 240401 (2002)
58. S.P. Walborn, D.S. Lemelle, M.P. Almeida, P.H.S. Ribeiro, Phys. Rev. Lett. **96**, 090501 (2006), http://link.aps.org/abstract/PRL/v96/e090501
59. N. González, G. Molina-Terriza, J.P. Torres, Opt. Express **14**, 9093 (2006), http://www.opticsinfobase.org/abstract.cfm?URI=oe-14-20-9093
60. H. Wei, X. Xue, J. Leach, M.J. Padgett, S.M.Barnett, S. Franke-Arnold, E. Yao, J. Courtial, Opt. Commun. **223**, 117 (2003)
61. J. Courtial, D.A. Robertson, K. Dholakia, L. Allen, M.J. Padgett, Phys. Rev. Lett. **81**, 4828 (1998)
62. J. Leach, J. Courtial, K. Skeldon, S.M. Barnett, S. Franke-Arnold, M.J. Padgett, Phys. Rev. Lett. **92**, 13601 (2004)
63. G. Whyte, J. Veitch, P. Öhberg, J. Courtial, Phys. Rev. A **70**, 011603 (2004)
64. A. Einstein, Annalen der Physik **17**, 891 (1905), http://adsabs.harvard.edu/abs/2005AnP....14S.194E
65. A. Einstein, B. Podolsky, N. Rosen, Phys. Rev. **47**, 777 (1935)
66. J.S. Bell, Physics **1**, 195 (1964)
67. J.F. Clauser, M.A. Horne, A. Shimony, R.A. Holt, Phys. Rev. Lett. **23**, 880 (1969)
68. A. Aspect, P. Grangier, G. Roger, Phys. Rev. Lett. **47**, 460 (1981), http://link.aps.org/abstract/PRL/v47/p460
69. A. Aspect, P. Grangier, G. Roger, Phys. Rev. Lett. **49**, 91 (1982), http://link.aps.org/abstract/PRL/v49/p91
70. A. Aspect, J. Dalibard, G. Roger, Phys. Rev. Lett. **49**, 1804 (1982)
71. G. Weihs, T. Jennewein, C. Simon, H. Weinfurter, A. Zeilinger, Phys. Rev. Lett. **81**, 5039 (1998), http://link.aps.org/abstract/PRL/v81/p5039
72. A. Aspect, Nature **398**, 189 (1999)
73. D. Kaszlikowski, P. Gnaciński, M.Żukowski, W. Miklaszewski, A. Zeilinger, Phys. Rev. Lett. **85**, 4418 (2000), http://link.aps.org/abstract/PRL/v85/p4418
74. H.H. Arnaut, G.A. Barbosa, Phys. Rev. Lett. **85**, 286 (2000),
75. S. Franke-Arnold, S.M. Barnett, M.J. Padgett, L. Allen, Phys. Rev. A **65**, 033823 (2002), http://link.aps.org/abstract/PRA/v65/p33823
76. A. Vaziri, J.W. Pan, T. Jennewein, G. Weihs, A. Zeilinger, Phys. Rev. Lett. **91**, 227902 (2003)
77. S.S.R. Oemrawsingh, X. Ma, D. Voigt, A. Aiello, E.R. Eliel, G. 't Hooft, J.P. Woerdman, Phys. Rev. Lett. **95**, 240501 (2005)